

Elemental Stoichiometry of Particulate Organic Matter across the Atlantic Ocean

Adam J Fagan¹, Tatsuro Tanioka¹, Alyse A Larkin², Jenna Alyson Lee³, Nathan S Garcia⁴, and Adam Camillo Martiny¹

¹University of California, Irvine

²University of California Irvine

³Princeton University

⁴UC Irvine Earth System Science

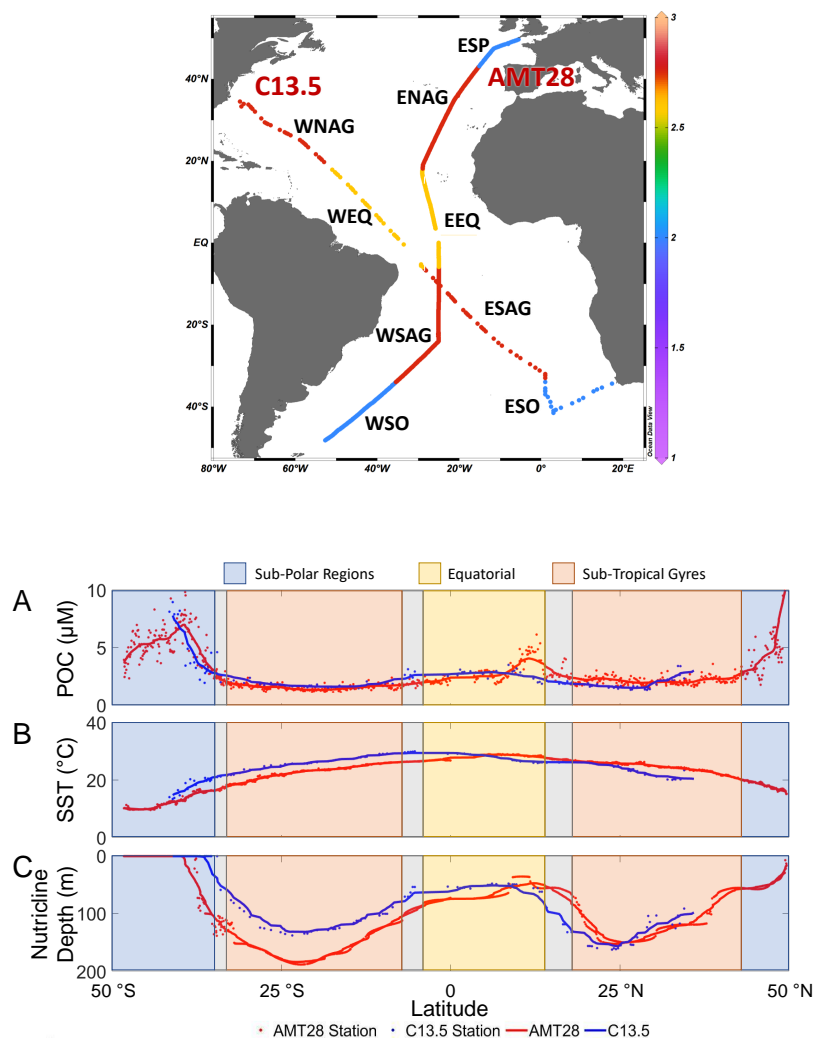
May 13, 2023

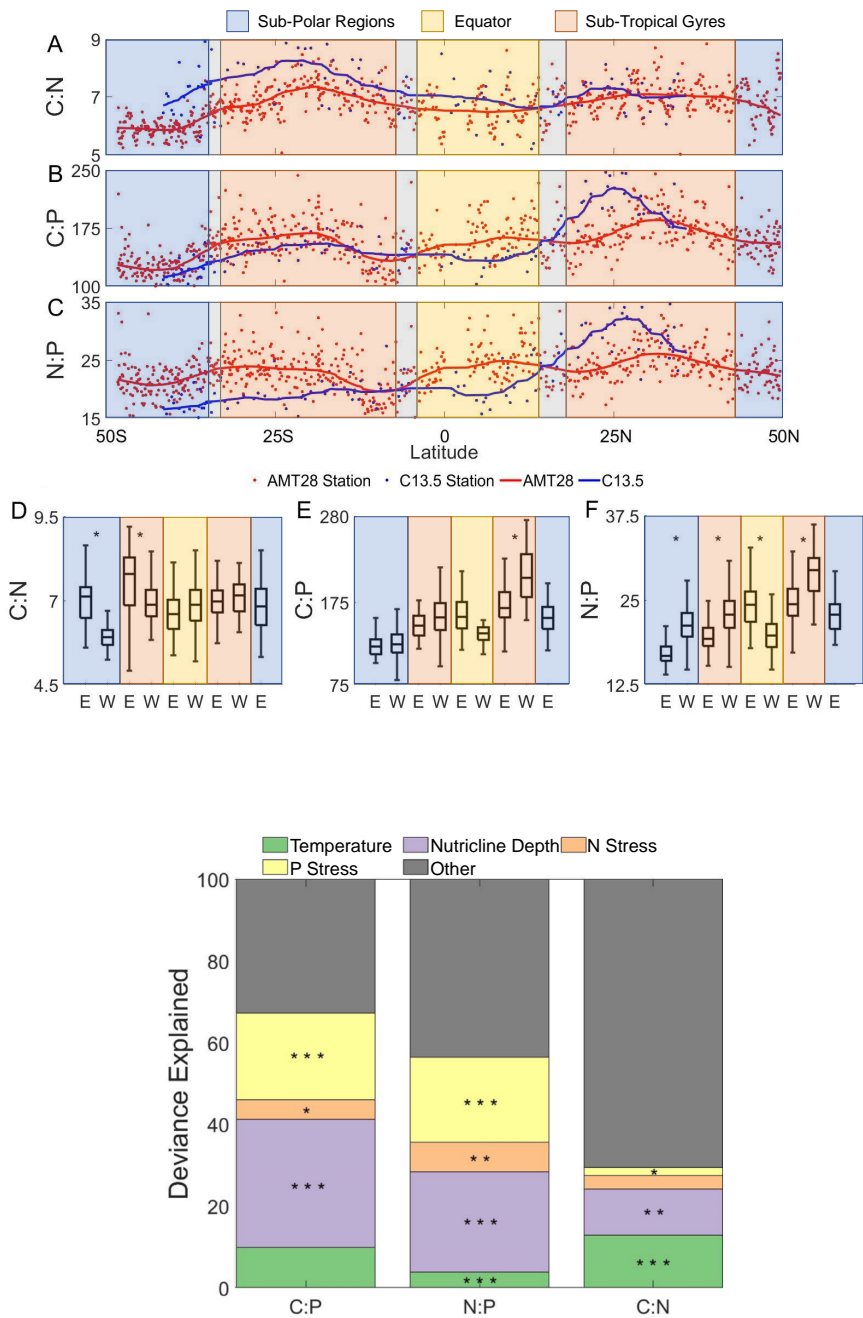
Abstract

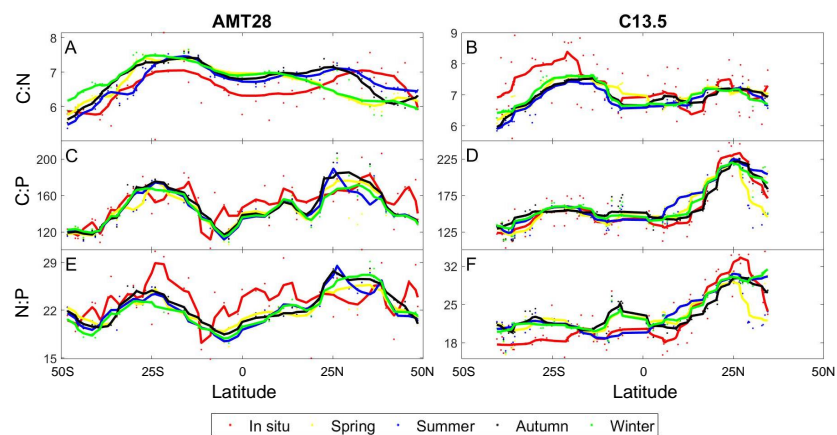
Recent studies show that stoichiometric elemental ratios of marine ecosystems are not static at Redfield proportions but vary systematically between biomes. However, the wider Atlantic Ocean is under-sampled for particulate organic matter (POM) elemental composition, especially as it comes to phosphorus. Thus, it is uncertain how environmental variation in this region translates into shifts in C:N:P. To address this, we analyzed hydrography, genomics, and POM concentrations from 877 stations on the meridional transects AMT28 and C13.5, spanning the Atlantic Ocean. We observed nutrient-replete, high-latitude ecosystem C:N:P to be significantly lower than the oligotrophic gyres. Latitudinal and zonal differences in elemental stoichiometry were linked to overall nutrient supply as well as N vs. P limitation. C:P and N:P were generally higher in the P-stressed northern region compared to southern hemisphere regions. We also detected a zonal difference linked to a westward deepening nutricline and a shift from N to P limitation. We also evaluated possible seasonal changes in C:N:P across the basin and predicted these to be limited. Overall, this study confirms latitudinal shifts in surface ocean POM ratios but reveals previously unrecognized hemisphere and zonal gradients. This work demonstrates the importance of understanding how regional shifts in hydrography and type of nutrient stress shape the coupling between Atlantic Ocean nutrient and carbon cycles.

Hosted file

961980_0_art_file_10966436_rwb3d2.docx available at <https://authorea.com/users/610908/articles/642676-elemental-stoichiometry-of-particulate-organic-matter-across-the-atlantic-ocean>







Hosted file

961980_0_supp_10929895_rt7jn4.docx available at <https://authorea.com/users/610908/articles/642676-elemental-stoichiometry-of-particulate-organic-matter-across-the-atlantic-ocean>

Elemental Stoichiometry of Particulate Organic Matter across the Atlantic Ocean

Adam J. Fagan¹, Tatsuro Tanioka¹, Alyse A. Larkin¹, Jenna A. Lee¹, Nathan S. Garcia¹, & Adam C. Martiny^{1,2,*}

¹Department of Earth System Science, University of California, Irvine, CA, USA

²Department of Ecology and Evolutionary Biology, University of California, Irvine, CA, USA

*Corresponding Author: amartiny@uci.edu

Abstract:

Recent studies show that stoichiometric elemental ratios of marine ecosystems are not static at Redfield proportions but vary systematically between biomes. However, the wider Atlantic Ocean is under-sampled for particulate organic matter (POM) elemental composition, especially as it comes to phosphorus. Thus, it is uncertain how environmental variation in this region translates into shifts in C:N:P. To address this, we analyzed hydrography, genomics, and POM concentrations from 877 stations on the meridional transects AMT28 and C13.5, spanning the Atlantic Ocean. We observed nutrient-replete, high-latitude ecosystem C:N:P to be significantly lower than the oligotrophic gyres. Latitudinal and zonal differences in elemental stoichiometry were linked to overall nutrient supply as well as N vs. P limitation. C:P and N:P were generally higher in the P-stressed northern region compared to southern hemisphere regions. We also detected a zonal difference linked to a westward deepening nutricline and a shift from N to P limitation. We also evaluated possible seasonal changes in C:N:P across the basin and predicted these to be limited. Overall, this study confirms latitudinal shifts in surface ocean POM ratios but reveals previously unrecognized hemisphere and zonal gradients. This work demonstrates the importance of understanding how regional shifts in hydrography and type of nutrient stress shape the coupling between Atlantic Ocean nutrient and carbon cycles.

29 **Plain Language Summary:**

30 Climate change is anticipated to influence the biological pump by altering phytoplankton nutrient
31 distribution. In our research, we conducted comprehensive measurements of particulate matter
32 concentrations during two large oceanographic field studies. We observed systematic variations
33 in organic matter concentrations and ratios across the Atlantic Ocean, both latitudinally and
34 longitudinally. Through statistical modeling, we determined that these variations are associated
35 with differences in the availability of essential nutrients for phytoplankton growth. Our findings
36 highlight the adaptive resource utilization among surface ocean plankton, which in turn
37 modulates the interplay between the ocean's nutrient and carbon cycles.
38

39 **Key Points:**

- 40 • There was systematic regional variation in POM concentrations and ratios across the
41 Atlantic Ocean.
- 42 • Latitudinal variability in C:N:P is linked to the nutrient supply rate and N vs P limitation.
- 43 • Westward deepening isopycnals and nutricline and shift from N to P limitation
44 correspond to zonal variability in C:N:P.
45

1. Introduction

Climate change is expected to impact the efficiency of the biological pump via changes in phytoplankton nutrient allocation and C:N:P. However, the impact of ocean warming on efficiency remains uncertain, with potential consequences for both ecosystems and the global carbon cycle (Kwon et al., 2022). Over the past few decades, studies have observed variability in marine plankton and ecosystem elemental composition (Martiny, Pham, et al., 2013; Martiny, Vrugt, et al., 2013; Weber & Deutsch, 2010). Specifically, regions with nutrient-rich conditions have lower C:N:P ratios (equatorial, coastal, and polar regions), and nutrient-poor conditions (subtropical gyre regions) have higher ratios (Martiny, Pham, et al., 2013; Martiny, Vrugt, et al., 2013). However, data compilations include variations in both sampling and analysis methods (Martiny et al., 2014) as well as have limited spatial coverage. Therefore, large-scale sampling efforts like Bio-GO-SHIP are quantifying ecosystem particulate organic matter (POM) concentrations and their elemental ratios utilizing consistent methodology on a global scale (Clayton et al., 2022; Tanioka et al., 2022).

Bio-GO-SHIP cruises have been limited to the Indian (Garcia et al., 2018) and the Pacific Ocean (Lee et al., 2021) and so far, lack coverage for much of the Atlantic Ocean. Local studies at the Bermuda Atlantic Time-series (BATS) site or short transects around the western North Atlantic Ocean show an N:P ratio up to 40-50 and C:N near Redfield proportions (Babiker et al., 2004; Cavender-Bares et al., 2001; Michaels et al., 1994; Michaels & Knap, 1996; Steinberg et al., 2001). In contrast, POM dynamics and especially N:P and C:P ratios are less understood for other regions, including the under-sampled South Atlantic Ocean. Greater spatial coverage of POM measurements, both latitudinally and longitudinally, is needed to understand the coupled elemental cycles in the Atlantic Ocean.

The Atlantic Ocean has a unique dynamic with phosphorus limitations north of and nitrogen limitations south of the equator (Cotner et al., 1997; Mather et al., 2008). In P-limited regions, N:P and C:P are often elevated from frugal P use (Galbraith & Martiny, 2015). In support, the well-sampled NW Atlantic Ocean displays high N:P and C:P (Lomas et al., 2010; Lomas et al., 2022). N limitation is more widespread in the South Atlantic Ocean, but no study has quantified ecosystem C:N:P here (Mather et al., 2008; Ustick et al., 2021). Temperature and other environmental factors are also important for C:N:P variability (Yvon-Durocher et al., 2015; Moreno and Martiny, 2018), but how such environmental variation affects the Atlantic Ocean elemental stoichiometry is unknown. Therefore, the broad environmental gradients in the Atlantic Ocean could result in significant regional ecosystem C:N:P shifts.

Here, we quantified suspended particulate organic carbon, nitrogen, and phosphorus concentrations along two Bio-GO-SHIP meridional transects: AMT 28 and C13.5 (Fig. 1), covering large parts of the Atlantic Ocean. We addressed three questions: (1) What are meridional, hemispheric, and zonal differences in POM concentrations and stoichiometry? and (2) What is the relationship between environmental factors and C:N:P? We hypothesize that differences in total nutrient supply and temperature are primarily responsible for the latitudinal gradient in C:N:P. In contrast, the type of nutrient limitation will be important for hemispheric and longitudinal C:N:P shifts.

2. Methods

2.1. Cruise Transects

AMT28 started in Harwich, UK (49°38'N/5°30'W), and ended in Mare Harbour, Falkland Islands (48°12'S/52°42'W), departing on September 25, 2018 and ending on October 27, 2018. C13.5 started in Cape Town, South Africa (34°22'S/17°18'W), and ended in Norfolk, VA (36°5'N/74°34'W), departing on March 21, 2020, and ending on April 16, 2020. C13.5 was set to go into the Southern Ocean and collect samples along the Eastern boundary of the South Atlantic Ocean. Due to COVID-19 quarantine restrictions, it was redirected to a port in Virginia. Fortuitously, this redirect allowed sample collection across the eastern South Atlantic Ocean and the western North Atlantic Ocean.

2.2. Sample Collection

Seawater for the POM was collected from the underway flow-through system for both cruises at a depth of approximately 5 m. This method involved initially passing water through a 30 µm nylon mesh to remove the stochastic presence of large particles from the samples. We then collected 3-8 liters of filtered water in 8.5L plastic polycarbonate carboys (Thermo Fisher Scientific, Waltham, MA). The carboys were placed at a 45° angle to prevent particles from settling below the nozzle. Next, particulate organic carbon (POC), nitrogen (PON), and phosphorus (POP) samples were filtered onto 25 mm pre-combusted GF/F (500°C for 5 hours) (Whatman, Florham Park, NJ) (POC/PON on the same filter). POP filters were rinsed with 5ml of 0.17M Na₂SO₄ to remove traces of dissolved phosphorous from the filter. Finally, we stored all filters in pre-combusted aluminum packets and placed them in a -80°C freezer during the cruise, a -20°C cooler for shipping, and back to a -80°C freezer until analysis. Between sample collections, the carboys and tubing were rinsed with 30 µm filtered sample water just prior to collection.

We collected single samples of POC/PON and POP hourly for AMT28. For the C13.5 transect, POC/PON and POP samples were collected in triplicate every ~4 h hours. Water collection for C13.5 was done at the peak and trough of the diel cycle, ~0600 and ~2000, respectively, with a balance of collections in between to prevent bias in sample collection.

2.3. Particulate Organic Matter Determination

2.3.1. Particulate Organic Phosphorus (POP) Assay

POP was analyzed using a modified ash-hydrolysis protocol (Lomas et al., 2010). Filters were placed into acid-washed/pre-combusted glass vials with 2ml of 0.017 M MgSO₄ and covered with pre-combusted aluminum foil. The vials were then placed in an incubator for 24h at 80-90°C and then combusted for 2 h at 500°C. After cooling, 5 ml of 0.2 M HCl was added and incubated at 80-90°C for 30 min. The supernatant was collected, and the vials were rinsed with 5 ml of Milli-Q water. The rinse water was collected and added to the supernatant. 1 ml of mixed reagent (2:5:1:2 parts ammonium molybdate tetrahydrate (24.3 mM), sulfuric acid (5N), potassium antimonyl tartrate (4.1 mM), and ascorbic acid (0.3 M) was added to the supernatant and left in the dark for 30 minutes. Samples were analyzed on a spectrophotometer at a wavelength of 885nm using a potassium monobasic phosphate standard (1.0 mM-P). The detection limit for POP measurements was ~0.3 µg.

2.3.2. Particulate Organic Carbon/Nitrogen (POC/PON) Assay

POC/PON are measured using the same filter. The POC/PON samples were processed in the lab at UCI using a JGOFS protocol (Ducklow & Dickson, 1994). POC/PON samples were dried in an incubator at 55°C for 24 hours. They were then moved to a desiccator with concentrated HCl fumes for 24 hours to remove inorganic carbon. The samples were then re-dried at 55°C for 24 hours before being packaged into pre-combusted tin capsules (CE Elantech, Lakewood, NJ). The packaged filters were analyzed on a CN FlashEA 1112 Elemental Analyzer (Thermo Scientific, Waltham, MA) with atropine and acetanilide standards. POC and PON measurements had a detection limit of ~2.4 ug and ~3.0 ug. Settings for the FlashEA had an oxidative reactor temperature of 900°C, a reduction reactor temperature of 680°C, and an oven temperature of 50°C. Oxygen introduced to the oxidative reactor last seven seconds allowing temperatures to reach 1800°C for sample combustion. A leak test needed to fall below 5ml/min before samples were analyzed to minimize sample loss.

2.4. Nutrient Availability, Biogeography, and Biological Properties

2.4.1. Nutricline Depth

The nutricline depth was determined as the 1 µM nitrate depth horizon (Garcia et al., 2018). Nutricline depth was regarded as a proxy for nutrient supply to the surface, with a shallow nutricline representing a high flux of nutrients and vice-versa for deep nutricline. The nutricline depth with respect to the 1/16 µM phosphate depth horizon was also investigated but found to be nearly identical to that of nitrate. For AMT28, nitrate concentrations were quantified as previously described from CTD casts along the transect (Swift, 2019). Nitrate concentrations were then interpolated using DIVA implemented in Ocean Data View (v5.5.2) (Schlitzer, 2019). For C13.5, we used the seasonal average nitrate depth profiles from 2018 of the World Ocean Atlas at 1-degree spatial resolution to determine nutricline depths. This approach was necessary as the logistical issues related to COVID quarantine restrictions prevented us from collecting onboard CTD measurements. Linear interpolation for each profile within the 1-degree was performed to estimate the nutricline depth.

2.4.2. Delineation of Regions

The regions under consideration for this study are the Eastern Subpolar (ESP) [Lat. 49.6°N-43.2°N] Western North Atlantic Gyre (WNAG) [Lat. 34.5°N-19.8°N], Eastern North Atlantic Gyre (ENAG) [Lat. 43.0°N-18.1°N], Western Equatorial (WEQ) [Lat. 17.9°N-5.9°S], Eastern Equatorial (EEQ) [Lat. 17.8°N-5.9°N], Western South Atlantic Gyre (WSAG) [Lat. 6.0°S-34.0°S], Eastern South Atlantic Gyre (ESAG) [Lat. 6.2°S-33.0°S], Western Southern Ocean (WSO) [Lat. 34.1°S-48.2°S], and Eastern Southern Ocean (ESO) [Lat. 33.9°S-41.5°S] (Fig. 1). These boundaries are determined using inflection points along the nutricline depth and the temperature profile.

2.4.3. Cell Size

Cell size was based on flow cytometry samples collected during CTD casts (AMT28) at the top 200 m of the water column (Moreno et al., 2022). Flow cytometry samples (63 stations, 755 samples) were co-collected with the POM samples used in this study. Conversion of cell count to biomass (fg C/cell) was done following the methodology from Moreno et al., 2022. Briefly,

photoautotrophs were categorized into *Prochlorococcus*, *Synechococcus*, pico-eukaryotes, nano-eukaryotes, *Coccolithophore*, and *Cryptophytes*. Each cell type had a specific conversion factor in determining its biomass. Using a Monte Carlo approach, 95% confidence interval around cell size was determined using a normal distribution based on the mean and standard deviation. Then, a randomly chosen conversion factor was applied to each type. Allowing for 1000 runs, we estimate a 95% confidence interval (Moreno et al., 2022).

2.4.4. Metagenomics-Informed Nutrient Limitation

Element-specific nutrient stress was used from the global genome content of *Prochlorococcus* (Ustick et al., 2021). The described metagenomic samples (276) were co-collected with the POM samples used in this study. Based on variation in *Prochlorococcus* population gene content, we identified genes associated with N and P nutrient stress types. Briefly, gene index, or the severity of the nutrient stress, is quantified by calculating the frequency of nutrient acquisition genes within *Prochlorococcus* single-copy core genes and attributes the frequency to the genetic adaptation for overcoming nutrient stress type and severity. Although based on *Prochlorococcus*, there is a significant overlap between this genetic index of nutrient limitation and both Earth System Models and whole community nutrient addition assays (Ustick et al., 2021). Of the different intensities and types of stress, our study utilized data with gene information representing the most severe form of nutrient gene index for nitrogen and phosphorus stress.

2.5. Data Analysis

Data analysis was conducted using Matlab R2021b (MathWorks). An ANOVA analysis with a posthoc Tukey test was used to determine the relationship between the selected regions for environmental conditions and POM. The C:N:P ratios underwent a log transformation to achieve a normal distribution before the ANOVA analysis (Isles, 2020). Using R ver. 4.1.2 (R Core Team, 2021), we used generalized additive models (GAM) with package *mgcv* (v1.8) (Wood, 2017) to explain the strength of four variables in determining C:N:P (temperature, nutricline depth, nitrogen stress, and phosphorus stress).

3. Results

POM concentrations, temperature, and nutricline profiles were characteristic to each oceanographic region. POC, PON, and POP concentration were moderately correlated ($r = 0.45$, 0.48 , and 0.49 , respectively; $p < 0.001$) and showed overall similar biogeography (Fig. 2A and S1). All POM pools had peak concentrations at high latitudes, troughs in the subtropical gyres, and intermediate concentrations at the equator. In high latitude subpolar regions (WSO, ESO, and ESP), POC (and overall POM) was significantly elevated ($4.6\text{--}5.3\text{ }\mu\text{M}$; $p < 0.05$) compared to all other regions (EQ: $2.8\text{ }\mu\text{M}$, Gyre: $1.6\text{--}2.1\text{ }\mu\text{M}$) (Fig. 2A, Fig. S2). POM concentrations also showed a zonal difference. There were higher concentrations of POM in the western compared to the eastern region of the Southern Ocean, whereas the opposite was seen in the subtropical gyres (Fig. 2A and Fig. S2). At $\sim 10^\circ\text{S}$, C13.5 and AMT28 cross paths. We observed nearly identical POM concentrations (and ratios), suggesting a stable POM level despite sampling in different seasons. Temperature peaked equatorially ($\sim 28^\circ\text{C}$) for both transects and declined with increasing latitudes (Fig. 2B). We observed minor variation in the meridional temperature profile linked to the difference in the seasonal timing for each cruise leading to a slight southward shift in peak temperature during C13.5. Nutricline profiles for both transects were similar, with the deepest nutricline in the gyres and shallowest at high latitudes and the equator (Fig. 2C). Zonal variability in the nutricline depth was apparent, with the deepest values in the western ($135\text{--}150\text{ m}$) compared to the eastern side of the gyres ($114\text{--}116\text{ m}$). Thus, we observed a robust meridional gradient in POM concentrations and environmental conditions but also a zonal gradient in nutricline depth in the oligotrophic subtropical gyres.

We observed distinct latitudinal, zonal, and hemispheric C:N:P variability (Fig. 3). First, we detected peak ratios in the subtropical gyres, troughs in the high latitudes, and intermediate values at the equator for C:N, C:P, and N:P, matching patterns seen globally (Martiny, Pham et al., 2013). In the subtropical gyres, averaged C:N values were noticeably elevated ($7.0\text{--}7.6$) compared to the other regions (Sub-Polar: $6.0\text{--}7.2$, EQ: $6.6\text{--}6.8$) (Fig. 3A). C:P followed the same trend as C:N, with subtropical gyre regions being higher ($148\text{--}208$) than the other regions (Sub-Polar: $122\text{--}158$, EQ: $136\text{--}161$) (Fig. 3B). N:P showed parallel changes to C:P except the South Atlantic Gyre showing a N:P range encompassing those of all other regions ($20.1\text{--}29.2$) (Fig. 3C). Second, a zonal gradient was detected, whereby C:N was higher in the Eastern South compared to the Western South Atlantic Ocean (Fig. 3D). However, this zonal gradient was not seen in other regions. C:P also showed an opposite zonal trend with higher values on the western side, albeit only significantly different in the northern hemisphere (Fig. 3E). N:P showed the highest zonal variation. This ratio was significantly higher on the western (21.4) vs. eastern (17.1) side of the South Atlantic Subtropical Gyre (Fig. 3F), converging at $\sim 10^\circ\text{S}$ and again elevated on the western (29.2) compared to the eastern part (24.8) of the North Atlantic Subtropical Gyre (Fig. 3F). Third, there was also a hemisphere bias, whereby C:P, and N:P were elevated in the northern hemisphere and C:N somewhat higher in the southern hemisphere. In summary, we saw clear latitudinal, zonal, and hemisphere gradients in C:N:P across the Atlantic Ocean.

These trends are further supported when investigating N^* at 200 m for AMT28. In the Northern Hemisphere, N^* remains a positive value until 10°N , where it becomes negative (Fig. S3). While N^* is positive, there is a larger N:P as phosphorus is the limiting nutrient. Once negative, this indicates nitrogen limitation, leading to a smaller N:P. When comparing N^* and N:P directly, there is only a weak correlation ($r = 0.19$, $p < 0.001$). Beyond the general increasing

value of both N* and N:P from the South to the North, the features of the two plots do not line up directly. Rather it would appear the N* has shifted South in the Northern Hemisphere by 10°, and vice versa in the Southern Hemisphere.

The influence of phytoplankton composition, temperature, nutricline depth, and metagenomically-assessed N and P stress were tested as drivers of stoichiometry (Fig. 4). Using flow cytometry cell counts, we were able to determine the concentration and total biomass of separate species of photoautotrophs at each station for AMT28. From this, *Prochlorococcus* was determined to make up >93% of the community in the subtropical gyres and equator, and over 50% of the total biomass. 67% of the northern sub-polar region community consisted of *Prochlorococcus* but only 10% of the biomass, and the Southern Ocean was the only region without *Prochlorococcus* being the most abundant at 12% of the community and 1% of the biomass (Fig. S4). The variation in phytoplankton composition correlated significantly, but weakly, to shifts in elemental composition ($r = 0.23$ $p < 0.05$). However, shifts in phytoplankton biodiversity did only replicate the overall latitudinal shifts in C:P but failed to capture the detailed transitions (Fig. S5). Thus, it was unclear how strongly shifting biodiversity impacted the elemental stoichiometry.

A general additive model (GAM) with temperature and various dimensions of nutrient availability captured 67% and 56% of the total deviance for C:P and N:P, respectively. For C:P, nutricline and phosphorus stress accounted for 53% of the total (31% and 21%, respectively). For N:P, nutricline and phosphorus stress accounted for 45% of the total (25% and 21%, respectively). We could explain less total deviance for C:N (30%), with the temperature being the most significant ($p < 0.001$). As both temperature and nutricline depth were strongly correlated with latitude, these two factors also explained the majority of the latitudinal variability of C:N:P. The remaining percentage that would explain the variation of stoichiometry may be factors not taken into consideration for this study. Nevertheless, a combination of temperature and nutrient stress described most of the stoichiometric variability in the Atlantic Ocean.

A zonal gradient in nutricline depth and metagenomically-assessed N and P stress matched C:N:P shifts (Fig. 3D-F). Nutricline depth was significantly deeper ($p < 0.05$) in the western part of subtropical gyres in both hemispheres (Fig. S2). Furthermore, there was a westward shift from N towards P limitation (Fig. S6). This zonal shift in nutrient availability corresponds to a similar increase in C:P from 174 to 207 and N:P from 24.8 to 29.2 towards the western side of the oligotrophic gyres (Fig. 3E, F). In parallel, C:N showed the opposite trend declining from 7.6 on the eastern to 7.0 in the western side, matching a shift from N to P stress (Fig. 3D). GAM analyses conducted separately for western and eastern basins corroborated these observations highlighting that the relative importance of N vs. P stress (Fig. S7-9). In summary, zonal variability in nutrient stress, described by a westward deepening nutricline and increased P-stress, may regulate a zonal change in C:N:P.

We assessed the potential impact of seasonal environmental changes for C:N:P across the Atlantic Ocean. Seasonal environmental changes were characterized as shifts in nutricline depth and temperature, while assuming a stable biogeography of N vs. P stress (Fig. 5). As a control, we saw a significant correlation between the observed and predicted C:N:P for the season matching the cruise occurrence (Table S3). However, the statistical model did not predict high C:N in the eastern South Atlantic Ocean and overestimated N:P in the equatorial and western South Atlantic Ocean. C:N:P ratios were predicted to be mostly stable across seasons, although we detected shifts in C:N near the sub-tropical convergence zone reflecting an expansion and

contraction of oligotrophic conditions (Fig. 5A). However, C:P and N:P were predicted to be mostly stable. When assuming a stable biogeography of N and P stress zone, our statistical model predicted a mostly seasonally stable C:N:P across most of the Atlantic Ocean.

4. Discussion

There was clear latitudinal variability in POM concentrations and stoichiometry across the Atlantic Ocean. We detected a high POM concentration and low C:N:P at higher latitudes, low POM concentrations and high ratios in the subtropical gyres, and intermediate values near the equator. This meridional gradient in POM concentrations and ratios corresponded to parallel changes in nutricline depth and thus likely linked to the overall nutrient supply. Similar gradients in concentrations and ratios have been detected in the Indian Ocean (Garcia et al., 2018), the Pacific Ocean (Lee et al., 2021), and in a global synthesis (Martiny, Pham, et al., 2013). Thus, our new observations add further support to systematic biome shifts in C:N:P across major ocean basins.

High aeolian iron input to the North Atlantic Ocean supports the growth of nitrogen fixers, increases the N:P nutrient supply ratio, and causes widespread P stress (Capone, 2014; Schlosser et al., 2014; Ussher et al., 2013). Such P stress likely impacts the observed higher C:P and, to a lesser extent, N:P throughout much of the North Atlantic Ocean. POP has a minimum in the western North Atlantic Ocean (Fig. S1), suggesting that the parallel changes in N:P and C:P are caused by lower POP concentrations. In the South Atlantic Ocean, aeolian iron inputs are significantly lower, as most iron dust is washed out at the Intertropical Convergence Zone (Capone, 2014). Nitrogen fixation is hence suppressed (Wang et al., 2019), allowing most of the southern part to be partially nitrogen limited. This N limitation likely causes the depressed PON concentrations (Fig. S1) and elevated C:N but depressed N:P in much of the South Atlantic Ocean. Thus, the hemisphere deviation in C:N:P is hypothesized to be driven by a causal link between iron inputs, N₂-fixation, and shifts between N and P limitation (Martiny et al., 2019).

An additional zonal gradient in C:N:P may be linked to the westward deepening of the nutricline and a parallel shift from N towards P-limitation. P-limitation is detected throughout the central North Atlantic Ocean (Ustick et al., 2021), but both C:P and N:P are significantly higher on the western side. Using the nutricline depth as proxy, the nutrient flux appeared greater on the eastern side. In addition, aeolian nutrient inputs could relieve nutrient stress towards the east, suppressing C:P and N:P ratios (Garcia et al., 2018; Kremling & Streu, 1993; Mills et al., 2004; Neuer et al., 2004). The South Atlantic Ocean also has the east-west variability for C:N:P, although the gradient is highest for C:N. These zonal shifts in C:N:P can be explained by shallower nutricline depth and stronger N limitation in the eastern part and stronger P limitation in the western part of the South Atlantic Ocean (Ustick et al., 2021; Martiny et al., 2019). Thus, we observe important zonal variability in POM concentrations and their stoichiometric ratios, superimposed on the larger meridional and hemisphere gradients.

N and P-limitation are assessed based on genomic changes and adaptation in *Prochlorococcus* populations (Ustick et al., 2021). While additional genomic information can be added in the future, *Prochlorococcus* provides a starting point, as it is the most abundant and the majority of biomass for phytoplankton in the central Atlantic Ocean (Fig. S4) (Maranon et al., 2000; Zwirgmaier et al., 2007). Beyond the central Atlantic Ocean, *Prochlorococcus* is still found to be the most numerically abundant phytoplankton in the Eastern Sub-Polar regions, but biomass of other phytoplankton, with *Synechococcus* and Pico-Eukaryotes are having a larger contribution. The predicted restricted changes in seasonal values of C:N:P fall within the range

of those observed at BATS, where seasonal shifts in stoichiometry were similarly weak (Singh et al., 2015). The intersection point of the two transects (~10°S) also indicates minimal seasonal influence as the POM and stoichiometric values are similar despite collection in opposite seasons. While there is a temporal difference in sampling, predictive modeling suggests that the observed biogeography of C:N:P is stable in most of the central Atlantic Ocean, albeit with several exceptions. In summary, we detect clear meridional, hemisphere, and zonal gradients in elemental stoichiometry that corresponds to changes in nutrient supply and limitation type, but additional factors may affect regional shifts in C:N:P across the Atlantic Ocean.

Our POM concentration and elemental ratio observations from the Atlantic Ocean have implications for predicting future changes to the ocean carbon cycle. Recent models have suggested that C:N:P variability can ‘buffer’ the effects of stratification and reduced nutrient supply on primary productivity and carbon sequestration (Kwon et al., 2022, Tanioka and Matsumoto, 2017). Such models of C:N:P variability have so far been tied to the surface phosphorus concentration (Galbraith and Martiny, 2015). However, our observations from the Atlantic Ocean indicate that subtle shifts between N and P limitation can have additional impacts on the elemental stoichiometry. The dust deposition stimulation of N₂-fixation in the North Atlantic Ocean is likely responsible for part of the shift in nutrient stress type. This hemisphere variability suggests an additional role of iron supply in regulating C:N:P. Thus, climate change may alter future patterns of C:N:P as the perturbation of air-sea dynamics can modulate the strengths of boundary currents, the slope of a westward nutricline (Kelly et al., 2010), or the aeolian deposition of iron (Krishnamurthy et al., 2010). Such shifts in C:N:P could, in turn, have large impacts on global nitrogen fixation, primary production, or carbon sequestration.

Conflict of Interest

The authors declare no conflicts of interest relevant to this study.

Acknowledgments

We thank the Global Oceans Ship-Based Hydrographic investigations Program (GO-SHIP) and the Atlantic Meridional Transect Programme for facilitating this project. We extend a special thanks to Andrew Rees, Glen Tarren, and the crew of the *RSS James Clark* and Leticia Barbero and the crew of the *R/V Roger Revelle*. This research was funded by the National Science Foundation (OCE-1848576 and 1948842 to ACM), NASA (80NSSC21K1654 to ACM), NOAA (101813 Z7554214 to ACM), and Simons Postdoctoral Fellowship in Marine Microbial Ecology (724483 to TT). The PML AMT is funded by the UK Natural Environment Research Council through its National Capability Long-term Single Centre Science Program, Climate Linked Atlantic Sector Science (grant number NE/R015953/1). This study contributes to the international IMBeR project and is AMT contribution number XXX (number pending).

Data Availability Statement

The AMT data set presented here is publicly hosted by the British Oceanographic Data Centre (<https://doi.org/10.5285/b5900384-89f0-3a38-e053-6c86abc0409d>) (Larkin et al., 2020). Hydrographic data from the AMT28 transect are available (<https://cchdo.ucsd.edu/cruise/74JC20180923>) (Wimmer et al., 2019). The particulate organic matter data from the C13.5 transect are available here (<https://www.bco-dmo.org/dataset/868908>) (Martiny et al., 2022). Hydrographic data from C13.5 data are available (<https://cchdo.ucsd.edu/cruise/33RO20200321>). Nutricline depth for C13.5 is calculated from

401 gridded annual mean nitrate data from World Ocean Atlas 2018
402 (<https://www.ncei.noaa.gov/data/oceans/woa/WOA18/DATA/>) (NOAA, 2020).
403
404

Legends

Figure 1. Map of oceanographic cruise transects AMT28 (September 25 to October 27, 2018, n = 765) and C13.5 (March 21 to April 16, 2020, n = 112). Different oceanographic regions are separated using nutricline and temperature profiles (WSO = Western Southern Ocean, ESO = Eastern Southern Ocean, WSAG = Western South Atlantic Gyre, ESAG = Eastern South Atlantic Gyre, WEQ = Western Equatorial, EEQ = Eastern Equatorial, WNAG = Western North Atlantic Gyre, ENAG = Eastern North Atlantic Gyre, ESP = Eastern Subpolar). Colors delineate subpolar (blue), subtropical (red), and equatorial upwelling regions (yellow).

Figure 2. Meridional gradient in POC concentrations and environmental conditions for AMT28 (boreal fall) and C13.5 (boreal spring). (A) Averaged surface POC concentrations plotted according to latitude, (B) surface temperature, and (C) nutricline depth presented as $Z_{\text{nitrate}} > 1 \mu\text{M}$. The trend lines represent the moving average of samples for AMT28 (red/ n=50) and C13.5 (blue/ n=20) transects. Background colors indicate broad oceanographic regions separated by latitude (blue = Sub-Polar, red = Subtropical, yellow = Equatorial upwelling regions, grey = transition regions).

Figure 3. Latitudinal and regional shifts in POM stoichiometry. (A-C) Averaged observed surface C:N, C:P, and N:P. The trend lines represent the moving average of samples for AMT28 (red) and C13.5 (blue) transects. Linear regression line representative of all samples along the transects (black). (D-F) Regional C:N, C:P, and N:P represented by boxplots, where data were separated by latitude and longitude (E = East, W = West). Significant zonal (east-west) differences are denoted with * above plot based on Tukey posthoc significant difference test ($p = 0.05$). For all boxplots, a central black bar of the box represents the median value. The whiskers signify the range (min, max) of values excluding outliers.

Figure 4. Influence of environmental factors on stoichiometry. Stars indicate the significance of smooth terms used for Generalized Additive Models (GAM). *** = $p < 0.001$, ** = $p < 0.01$, * = $p < 0.05$. Green represents the influence of temperature, purple represents the influence of nutricline depth, orange represents the nitrogen stress, yellow represents the phosphorus stress, and grey represents the remaining factors of influence on the variability of C:N:P. N and P stress are reflective of the nutrient gene index, which is quantified by calculating the frequency of the nutrient acquisition genes within *Prochlorococcus* single-copy core genes. The frequency is attributed to the genetic adaptation for overcoming nutrient stress type and severity.

Figure 5. Predicted seasonal variability of stoichiometry across the Atlantic Ocean. Observed compared to predicted seasonal C:N for AMT28 (A) and C13.5 (B). Observed compared to predicted seasonal C:P for AMT28 (C) and C13.5 (D). Observed compared to predicted seasonal N:P for AMT28 (E) and C13.5 (F). Dots are discrete samples and the lines are moving averages over ten samples. AMT28 occurred during the fall 2018 and C13.5 during the spring 2020. In situ samples are red, predicted Spring is yellow, predicted Summer is blue, predicted Autumn is black, and predicted Winter is green.

References

- Babiker, I. S., Mohamed, M. A. A., Komaki, K., Ohta, K., & Kato, K. (2004). Temporal Variations in the Dissolved Nutrient Stocks in the Surface Water of the Western North Atlantic Ocean. *Journal of Oceanography*, 60(3), 553–562. <https://doi.org/10.1023/B:JOCE.0000038348.66907.db>
- Capone, D. G. (2014). An iron curtain in the Atlantic Ocean forms a biogeochemical divide. *Proceedings of the National Academy of Sciences*, 111(4), 1231–1232. <https://doi.org/10.1073/pnas.1322568111>
- Cavender-Bares, K. K., Karl, D. M., & Chisholm, S. W. (2001). Nutrient gradients in the western North Atlantic Ocean: Relationship to microbial community structure and comparison to patterns in the Pacific Ocean. *Deep Sea Research Part I: Oceanographic Research Papers*, 48(11), 2373–2395. [https://doi.org/10.1016/S0967-0637\(01\)00027-9](https://doi.org/10.1016/S0967-0637(01)00027-9)
- Clayton, S., Alexander, H., Graff, J. R., Poulton, N. J., Thompson, L. R., Benway, H., et al. (2022). Bio-GO-SHIP: The Time Is Right to Establish Global Repeat Sections of Ocean Biology. *Frontiers in Marine Science*, 8(767443). <https://doi.org/10.3389/fmars.2021.767443>
- Cotner, J., Ammerman, J., Peele, E., & Bentzen, E. (1997). Phosphorus-limited bacterioplankton growth in the Sargasso Sea. *Aquatic Microbial Ecology*, 13(2), 141–149. <https://doi.org/10.3354/ame013141>
- Ducklow, H., & Dickson, A. (1994). Shipboard sampling procedures. JGOFS. Retrieved from http://usjgofs.whoi.edu/JGOFS_19.pdf
- Galbraith, E. D., & Martiny, A. C. (2015). A simple nutrient-dependence mechanism for predicting the stoichiometry of marine ecosystems. *Proceedings of the National Academy of Sciences*, 112(27), 8199–8204. <https://doi.org/10.1073/pnas.1423917112>
- Garcia, C. A., Baer, S. E., Garcia, N. S., Rauschenberg, S., Twining, B. S., Lomas, M. W., & Martiny, A. C. (2018). Nutrient supply controls particulate elemental concentrations and ratios in the low latitude eastern Indian Ocean. *Nature Communications*, 9(1), 4868. <https://doi.org/10.1038/S41467-018-06892-w>
- Isles, P. D. F. (2020). The misuse of ratios in ecological stoichiometry. *Ecology*, 0(0), 1–7. <https://doi.org/10.1002/ecy.3153>
- Kelly, K. A., Small, R. J., Samelson, R. M., Qiu, B., Joyce, T. M., Kwon, Y. O., & Cronin, M. F. (2010). Western boundary currents and frontal air-sea interaction: Gulf stream and Kuroshio Extension. *Journal of Climate*, 23(21), 5644–5667. <https://doi.org/10.1175/2010JCLI3346.1>
- Kremling, K., & Streu, P. (1993). Saharan dust influenced trace element fluxes in deep North Atlantic subtropical waters. *Deep Sea Research Part I: Oceanographic Research Papers*, 40(6), 1155–1168. [https://doi.org/10.1016/0967-0637\(93\)90131-L](https://doi.org/10.1016/0967-0637(93)90131-L)
- Krishnamurthy, A., Moore, J. K., Mahowald, N., Luo, C., & Zender, C. S. (2010). Impacts of atmospheric nutrient inputs on marine biogeochemistry. *Journal of Geophysical Research*, 115(G1), G01006. <https://doi.org/10.1029/2009JG001115>
- Kwon, E. Y., Sreesh, M. G., Timmermann, A., Karl, D. M., Church, M. J., Lee, S.-S., & Yamaguchi, R. (2022). Nutrient uptake plasticity in phytoplankton sustains future ocean net primary production. *Science Advances*, 8(51), eadd2475. <https://doi.org/10.1126/sciadv.add2475>
- Larkin, A., Lee, J. A., & Martiny, A. (2020). Surface ocean particulate organic matter (POC, PON, and POP) from underway-collected samples along a north-south transect in the Atlantic Ocean on cruise AMT28/JR18001. British Oceanographic Data Centre, National

- Oceanography Centre, NERC, UK,. <https://doi.org/10.5285/b5900384-89f0-3a38-e053-6c86abc0409d>
- Lee, J. A., Garcia, C. A., Larkin, A. A., Carter, B. R., & Martiny, A. C. (2021). Linking a Latitudinal Gradient in Ocean Hydrography and Elemental Stoichiometry in the Eastern Pacific Ocean. *Global Biogeochemical Cycles*, 35(5). <https://doi.org/10.1029/2020GB006622>
- Lomas, M. W., Burke, A. L., Lomas, D. A., Bell, D. W., Shen, C., Dyhrman, S. T., & Ammerman, J. W. (2010). Sargasso Sea phosphorus biogeochemistry: An important role for dissolved organic phosphorus (DOP). *Biogeosciences*, 7(2), 695–710. <https://doi.org/10.5194/bg-7-695-2010>
- Lomas, M. W., Bates, N. R., Johnson, R. J., Steinberg, D. K., & Tanioka, T. (2022). Adaptive carbon export response to warming in the Sargasso Sea. *Nature Communications*, 13(1), 1211. <https://doi.org/10.1038/S41467-022-28842-3>
- Marañón, E., Holligan, P. M., Varela, M., Mouriño, B., & Bale, A. J. (2000). Basin-scale variability of phytoplankton biomass, production and growth in the Atlantic Ocean. *Deep Sea Research Part I: Oceanographic Research Papers*, 47(5), 825–857. [https://doi.org/10.1016/S0967-0637\(99\)00087-4](https://doi.org/10.1016/S0967-0637(99)00087-4)
- Martiny, A. C., Vrugt, J. A., Primeau, F. W., & Lomas, M. W. (2013). Regional variation in the particulate organic carbon to nitrogen ratio in the surface ocean. *Global Biogeochemical Cycles*, 27(3), 723–731. <https://doi.org/10.1002/gbc.20061>
- Martiny, A. C., Pham, C. T. A., Primeau, F. W., Vrugt, J. A., Moore, J. K., Levin, S. A., & Lomas, M. W. (2013). Strong latitudinal patterns in the elemental ratios of marine plankton and organic matter. *Nature Geoscience*, 6(4), 279–283. <https://doi.org/10.1038/ngeo1757>
- Martiny, A. C., Vrugt, J. A., & Lomas, M. W. (2014). Concentrations and ratios of particulate organic carbon, nitrogen, and phosphorus in the global ocean. *Scientific Data*, 1(1), 140048. <https://doi.org/10.1038/sdata.2014.48>
- Martiny, A. C., Lomas, M. W., Fu, W., Boyd, P. W., Chen, Y. L., Cutter, G. A., et al. (2019). Biogeochemical controls of surface ocean ocean phosphate. *Science Advances*, 5(8), eaax0341. <https://doi.org/10.1126/sciadv.aax0341>
- Martiny, A., Garcia, N. S., Tanioka, T., & Fagan, A. J. (2022). POM concentrations for carbon, nitrogen, and phosphorus from GO-SHIP Line C13.5/A13.5 in 2020. Biological and Chemical Oceanography Data Management Office (BCO-DMO). Version 1, Version Date 2022-01-31. <https://doi.org/10.26008/1912/bco-dmo.868908.1>
- Mather, R. L., Reynolds, S. E., Wolff, G. A., Williams, R. G., Torres-Valdes, S., Woodward, E. M. S., et al. (2008). Phosphorus cycling in the North and South Atlantic Ocean subtropical gyres. *Nature Geoscience*, 1(7), 439–443. <https://doi.org/10.1038/ngeo232>
- MATLAB:R2021b. (2021). (Version 9.11.0.1809720) (R2021b) [Software]. Natick, Massachusetts: The Mathworks, Inc.
- Michaels, A. F., & Knap, A. H. (1996). Overview of the U.S. JGOFS Bermuda Atlantic Time-series Study and the Hydrostation S program. *Deep Sea Research Part II: Topical Studies in Oceanography*, 43(2–3), 157–198. [https://doi.org/10.1016/0967-0645\(96\)00004-5](https://doi.org/10.1016/0967-0645(96)00004-5)
- Michaels, A. F., Knap, A. H., Dow, R. L., Gundersen, K., Johnson, R. J., Sorensen, J., et al. (1994). Seasonal patterns of ocean biogeochemistry at the U.S. JGOFS Bermuda Atlantic time-series study site. *Deep Sea Research Part I: Oceanographic Research Papers*, 41(7), 1013–1038. [https://doi.org/10.1016/0967-0637\(94\)90016-7](https://doi.org/10.1016/0967-0637(94)90016-7)
- Mills, M. M., Ridame, C., Davey, M., La Roche, J., & Geider, R. J. (2004). Iron and phosphorus

co-limit nitrogen fixation in the eastern tropical North Atlantic. *Nature*, 429(6989), 292–294. <https://doi.org/10.1038/nature02550>

Moreno, A. R., & Martiny, A. C. (2018). Ecological Stoichiometry of Ocean Plankton. *Annual Review of Marine Science*, 10(1), 43–69. <https://doi.org/10.1146/annurev-marine-121916-063126>

Moreno, A. R., Larkin, A. A., Lee, J. A., Gerace, S. D., Tarran, G. A., & Martiny, A. C. (2022). Regulation of the Respiration Quotient Across Ocean Basins [Dataset]. *AGU Advances*, 3(5), e2022AV000679. <https://doi.org/10.1029/2022AV000679>

Neuer, S., Torres-Padrón, M. E., Gelado-Caballero, M. D., Rueda, M. J., Hernández-Brito, J., Davenport, R., & Wefer, G. (2004). Dust deposition pulses to the eastern subtropical North Atlantic gyre: Does ocean's biogeochemistry respond? *Global Biogeochemical Cycles*, 18(4), n/a-n/a. <https://doi.org/10.1029/2004GB002228>

NOAA NCEI (2020), World Ocean Atlas 2018 data, National Centers for Environmental Information, <https://www.ncei.noaa.gov/data/oceans/woa/WOA18/DATA/> (Accessed August 9, 2020).

R Core Team. (2021). R: A Language and Environment for Statistical Computing. Vienna, Austria (Version 4.1.2) [Software]. Retrieved from <https://www.r-project.org/>

Schlitzer, R. (2019). Ocean Data View (Version 5.3.0) [Software]. Retrieved from <https://odv.awi.de>

Schlosser, C., Klar, J. K., Wake, B. D., Snow, J. T., Honey, D. J., Woodward, E. M. S., et al. (2014). Seasonal ITCZ migration dynamically controls the location of the (sub)tropical Atlantic biogeochemical divide. *Proceedings of the National Academy of Sciences of the United States of America*, 111(4), 1438–1442. <https://doi.org/10.1073/pnas.1318670111>

Sharoni, S., & Halevy, I. (2020). Nutrient ratios in marine particulate organic matter are predicted by the population structure of well-adapted phytoplankton. *Science Advances*, 6(29), eaaw9371. <https://doi.org/10.1126/sciadv.aaw9371>

Singh, A., Baer, S. E., Riebesell, U., Martiny, A. C., & Lomas, M. W. (2015). C : N : P stoichiometry at the Bermuda Atlantic Time-series Study station in the North Atlantic Ocean. *Biogeosciences*, 12(21), 6389–6403. <https://doi.org/10.5194/bg-12-6389-2015>

Steinberg, D. K., Carlson, C. A., Bates, N. R., Johnson, R. J., Michaels, A. F., & Knap, A. H. (2001). Overview of the US JGOFS Bermuda Atlantic Time-series Study (BATS): a decade-scale look at ocean biology and biogeochemistry. *Deep Sea Research Part II: Topical Studies in Oceanography*, 48(8–9), 1405–1447. [https://doi.org/10.1016/S0967-0645\(00\)00148-X](https://doi.org/10.1016/S0967-0645(00)00148-X)

Swift, J. (2019). CTD data from Cruise 74JC20180923. <https://doi.org/https://doi.org/10.7942/C2D08M>

Talmy, D., Martiny, A. C., Hill, C. N., Hickman, A. E., & Follows, M. J. (2016). Microzooplankton regulation of surface ocean POC:PON ratios. *Global Biogeochemical Cycles*, 30(2), 311–332. <https://doi.org/10.1002/2015GB005273>

Tanioka, T., Garcia, C. A., Larkin, A. A., Garcia, N. S., Fagan, A. J., & Martiny, A. C. (2022). Global patterns and predictors of C:N:P in marine ecosystems. *Communications Earth & Environment*, 3(1), 1–9. <https://doi.org/10.1038/s43247-022-00603-6>

Tanioka, T., & Matsumoto, K. (2017). Buffering of Ocean Export Production by Flexible Elemental Stoichiometry of Particulate Organic Matter. *Global Biogeochemical Cycles*, 31(10), 1528–1542. <https://doi.org/10.1002/2017GB005670>

Ussher, S. J., Achterberg, E. P., Powell, C., Baker, A. R., Jickells, T. D., Torres, R., & Worsfold,

P. J. (2013). Impact of atmospheric deposition on the contrasting iron biogeochemistry of the North and South Atlantic Ocean. *Global Biogeochemical Cycles*, 27(4), 1096–1107. <https://doi.org/10.1002/gbc.20056>

Ustick, L. J., Larkin, A. A., Garcia, C. A., Garcia, N. S., Brock, M. L., Lee, J. A., et al. (2021). Metagenomic analysis reveals global-scale patterns of ocean nutrient limitation [Dataset]. *Science*, 372(6539), 287–291. <https://doi.org/10.1126/science.abe6301>

Wang, W.-L., Moore, J. K., Martiny, A. C., & Primeau, F. W. (2019). Convergent estimates of marine nitrogen fixation. *Nature*, 566(7743), 205–211. <https://doi.org/10.1038/S41586-019-0911-2>

Weber, T. S., & Deutsch, C. (2010). Ocean nutrient ratios governed by plankton biogeography. *Nature*, 467(7315), 550–554. <https://doi.org/10.1038/nature09403>

Wimmer, W., Ballard, J., May, R., & Tarran, G. 2019. CTD data from Cruise 74JC20180923, exchange version. Accessed from CCHDO <https://cchdo.ucsd.edu/cruise/74JC20180923>. Access date 2019-11-14. CCHDO cruise DOI: 10.7942/C2D08M

Wood, S. N. (2017). *Generalized Additive Models* (Version 1.8) [Software]. Chapman and Hall/CRC. <https://doi.org/10.1201/9781315370279>

Yvon-Durocher, G., Dossena, M., Trimmer, M., Woodward, G., & Allen, A. P. (2015). Temperature and the biogeography of algal stoichiometry. *Global Ecology and Biogeography*, 24(5), 562–570. <https://doi.org/10.1111/geb.12280>

Zwirgmaier, K., Heywood, J. L., Chamberlain, K., Woodward, E. M. S., Zubkov, M. V., & Scanlan, D. J. (2007). Basin-scale distribution patterns of picocyanobacterial lineages in the Atlantic Ocean. *Environmental Microbiology*, 9(5), 1278–1290. <https://doi.org/10.1111/j.1462-2920.2007.01246.x>

[Data providers of the parameter(s) used]. [Year of file access]. [CTD/Bottle] data from cruise [expocode], [format version used]. Accessed from CCHDO [url of cruise data page]. Access date [date of download]. [Applicable CCHDO cruise DOI if provided].

2020. CTD data from Cruise 33RO20200321, exchange version. Accessed from CCHDO <https://cchdo.ucsd.edu/cruise/33RO20200321>. Access date 2020-08-09. CCHDO cruise DOI: 10.7942/C2894Z

Figure 1.

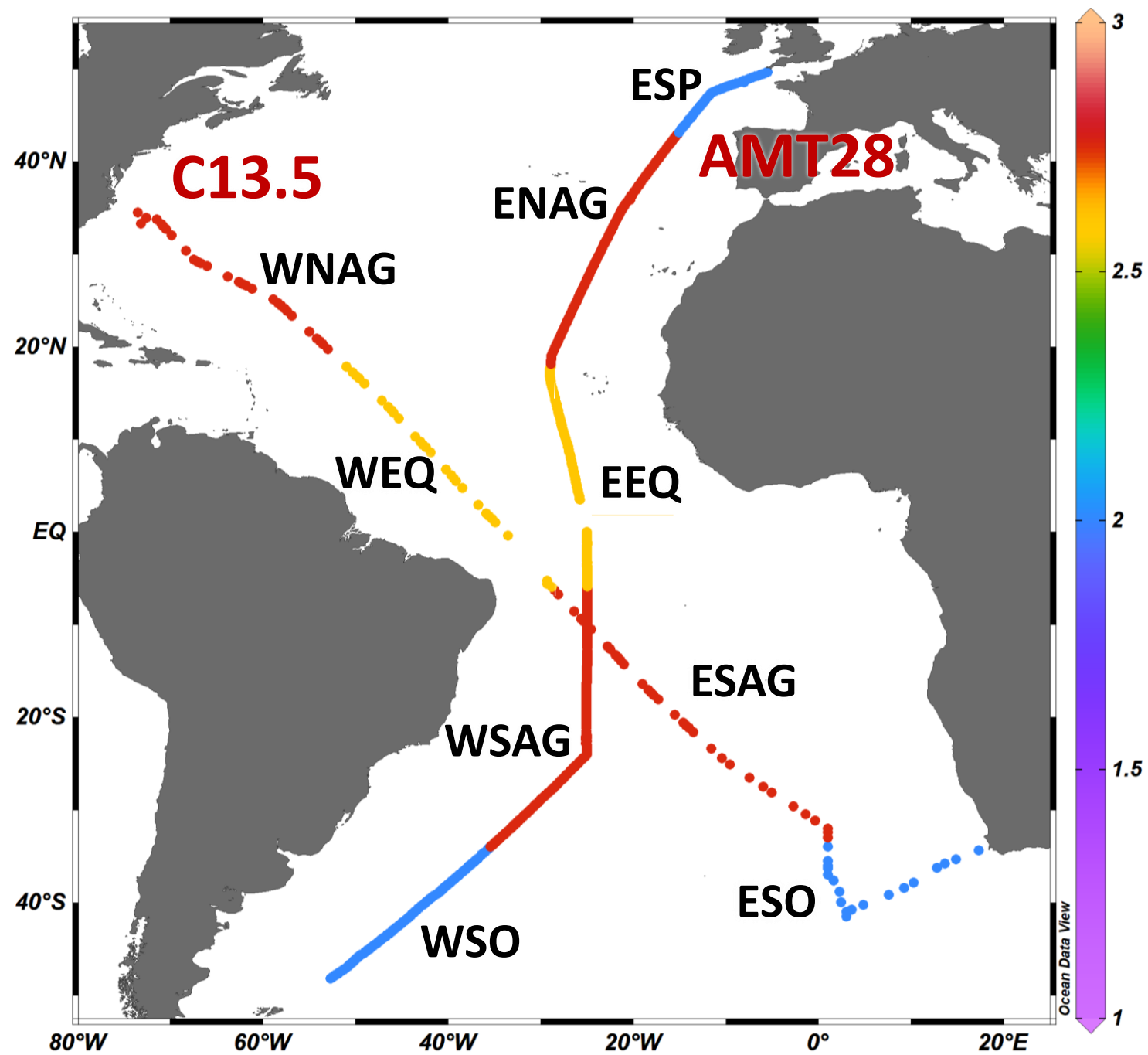


Figure 2.

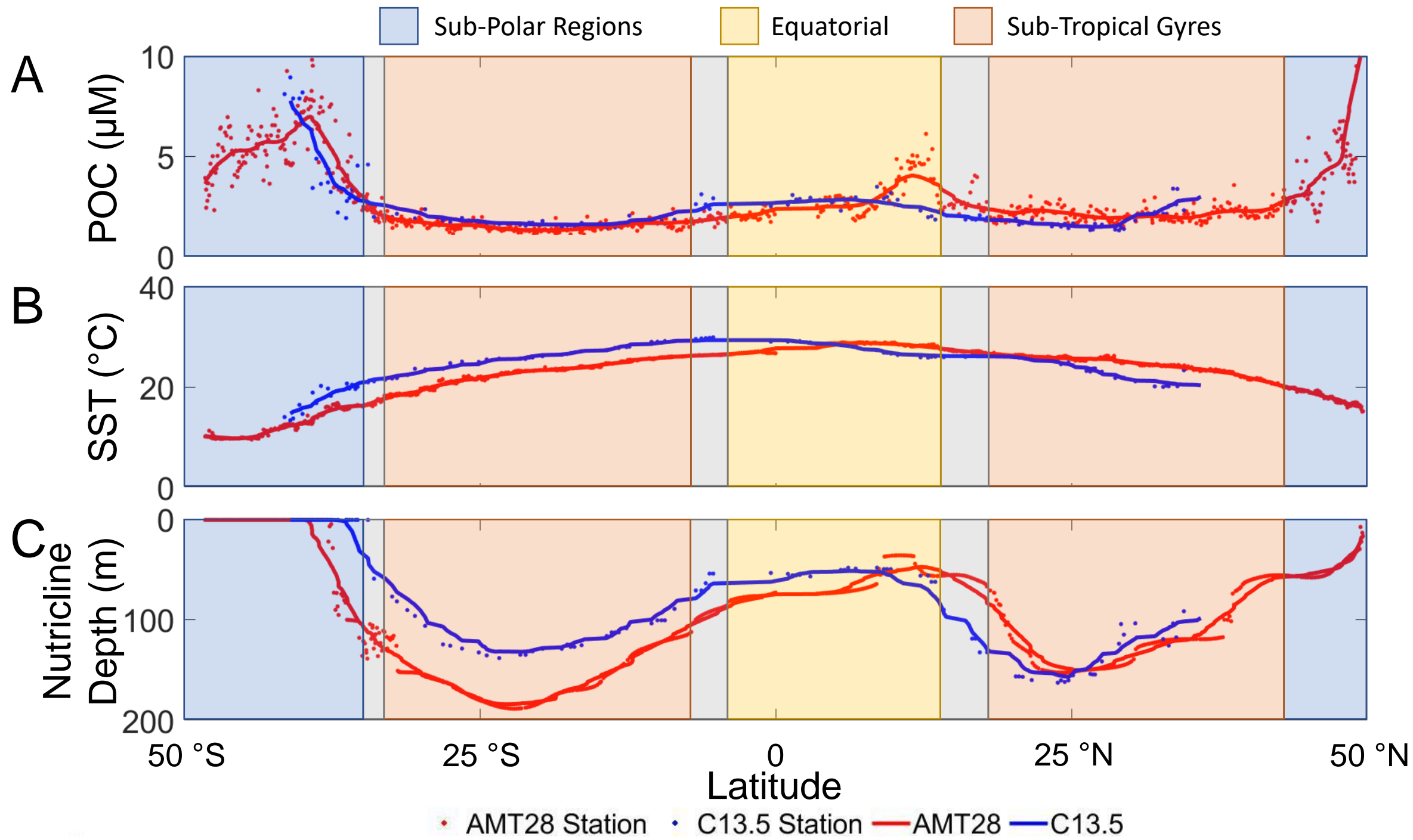


Figure 3.

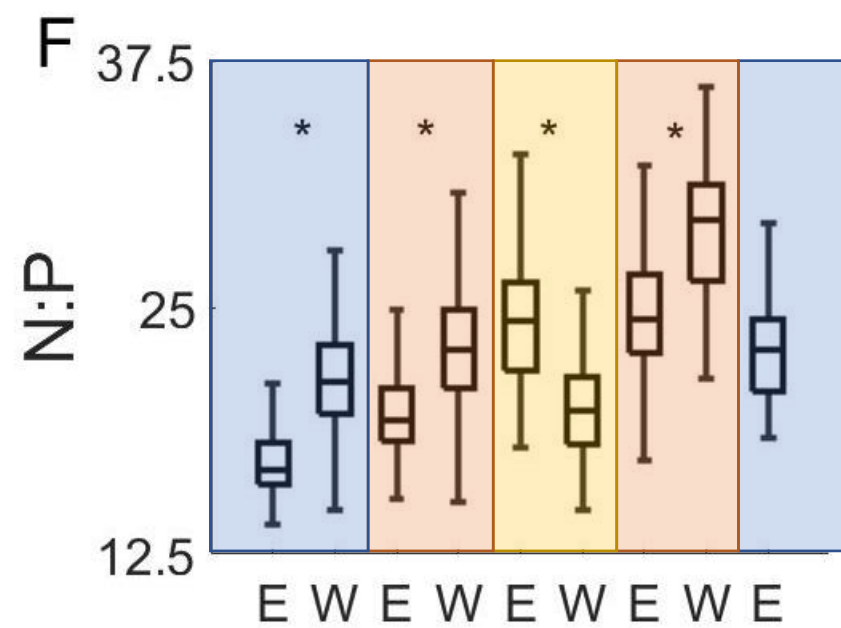
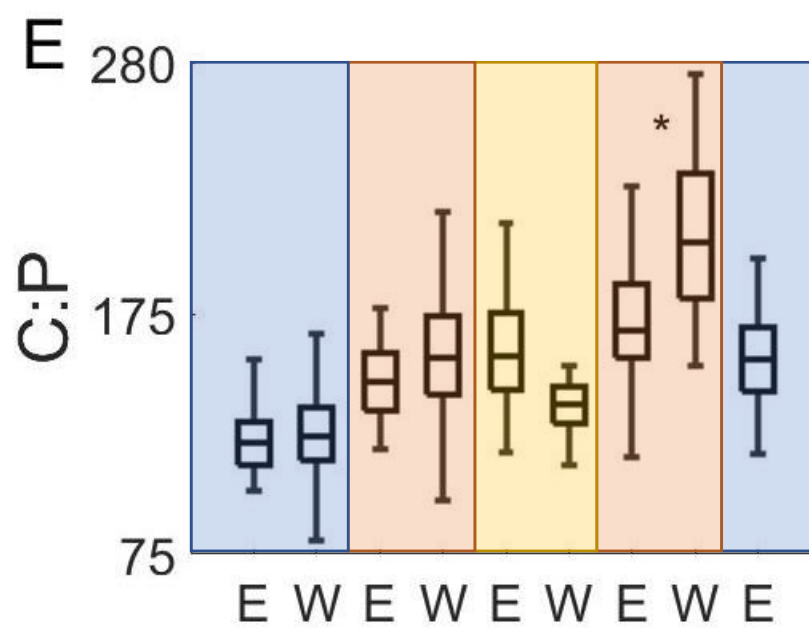
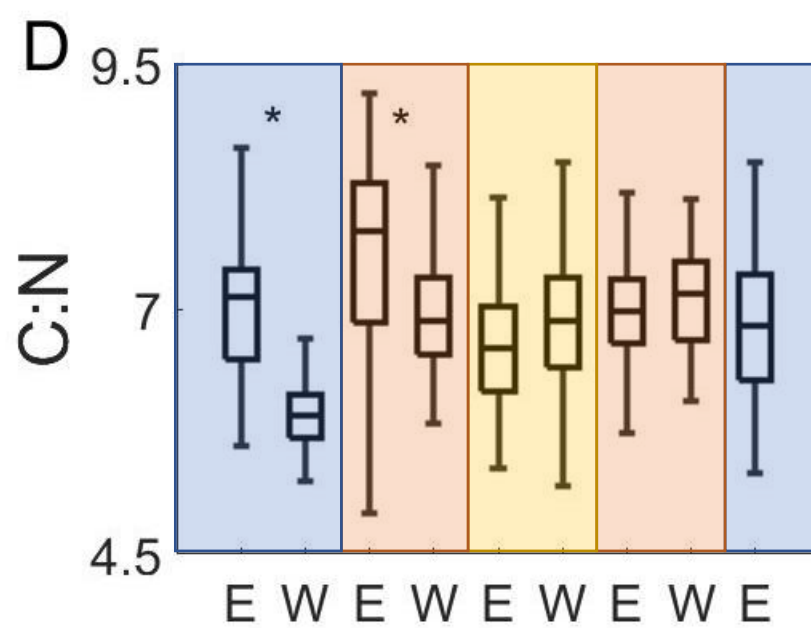
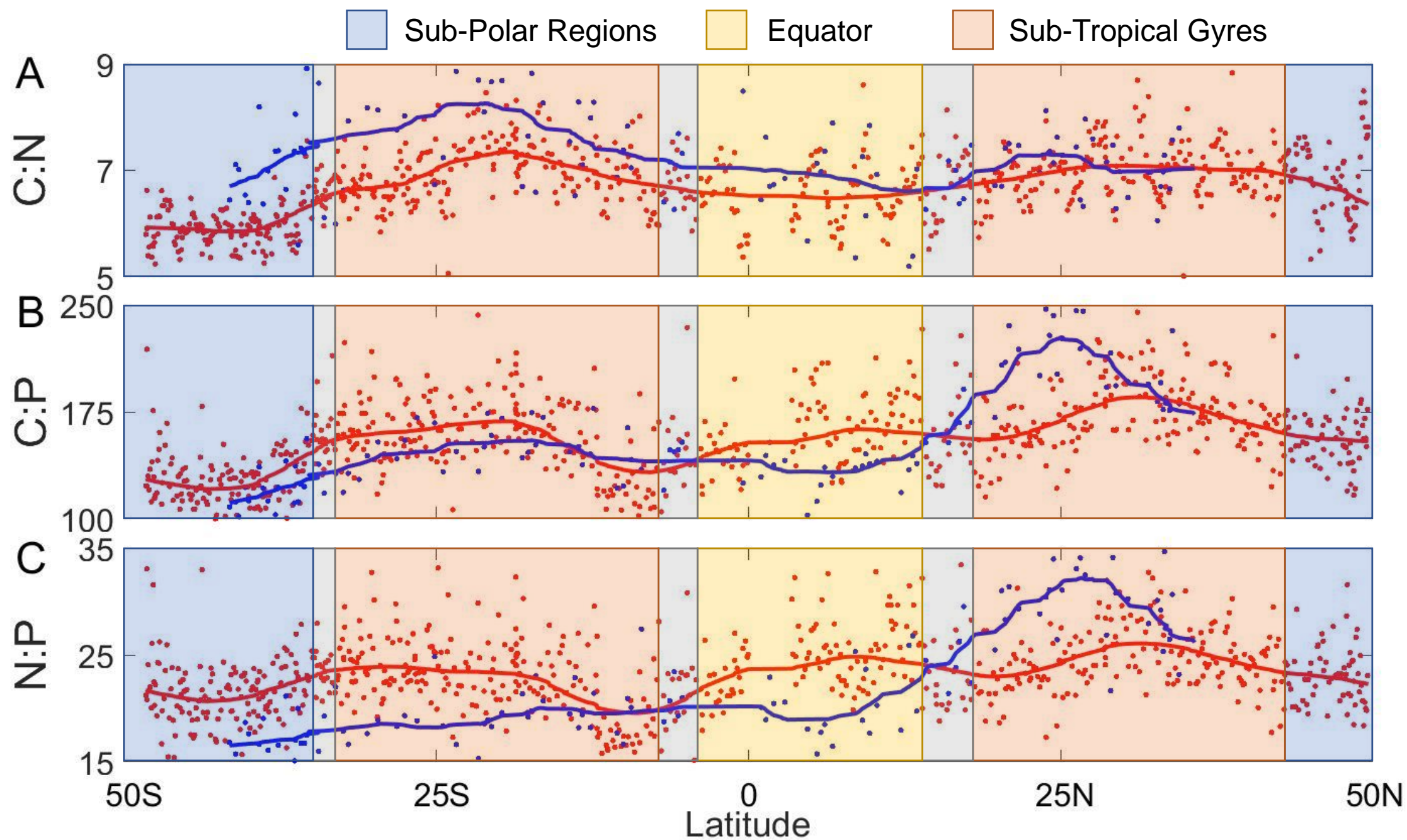


Figure 4.

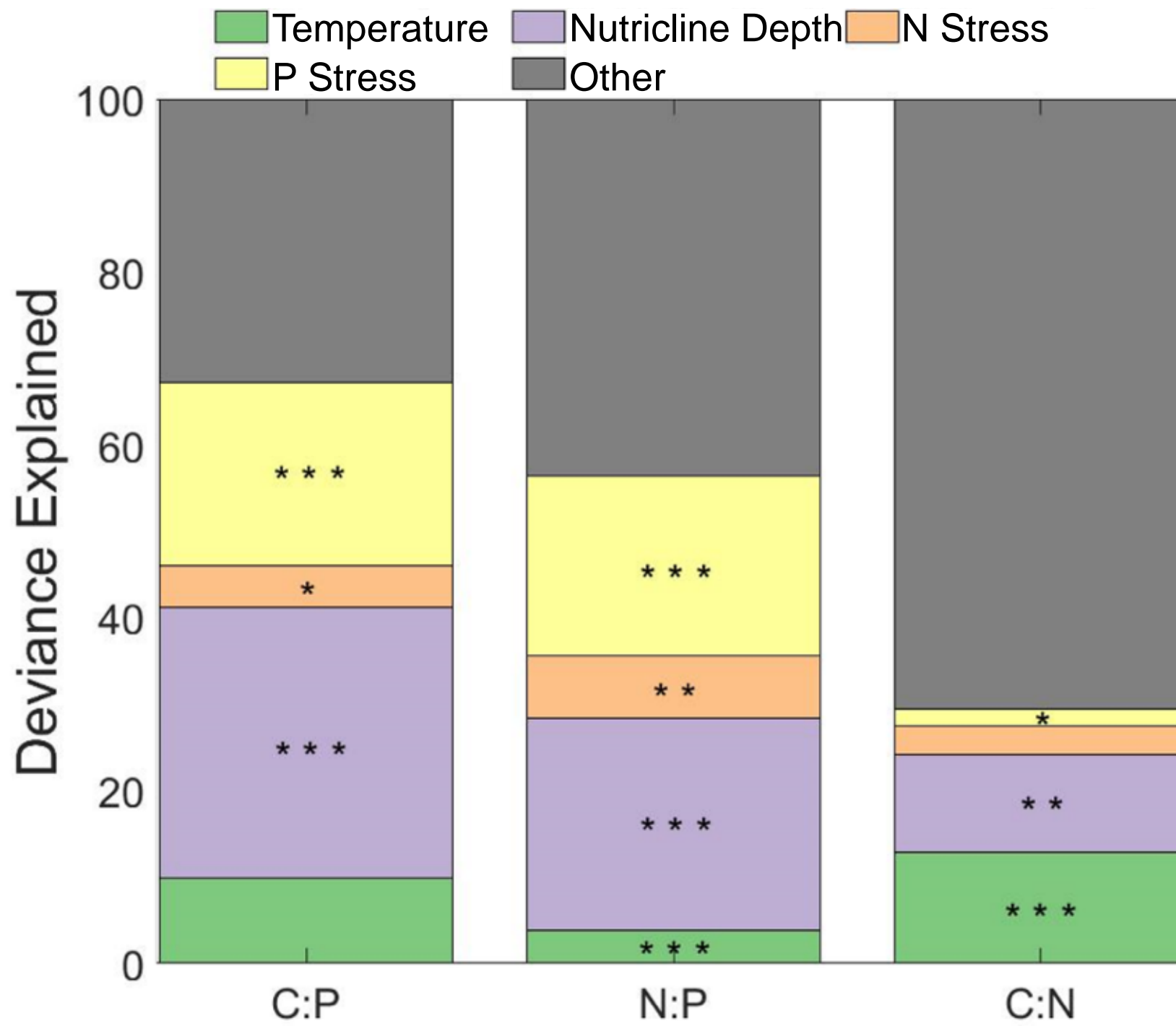
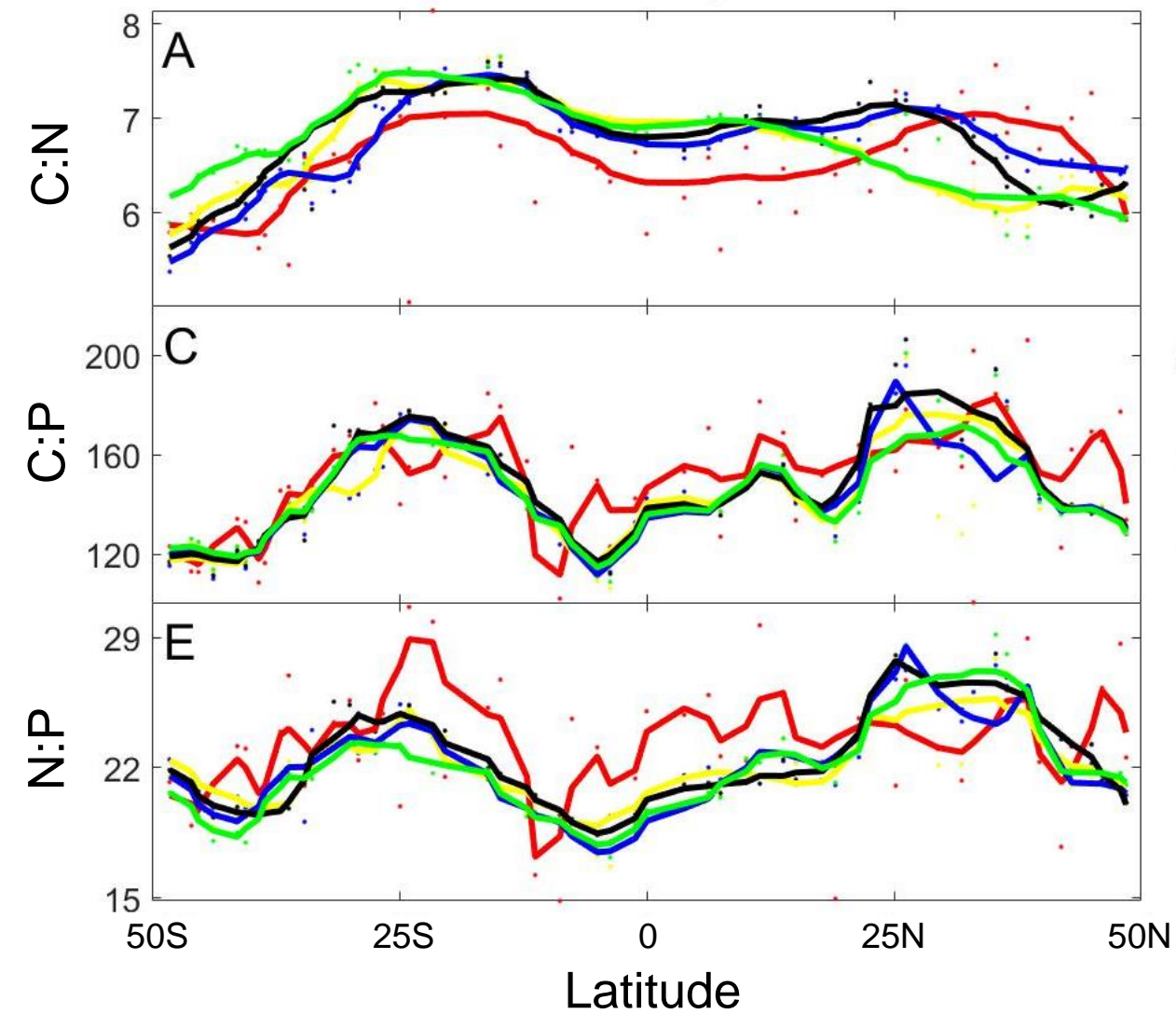
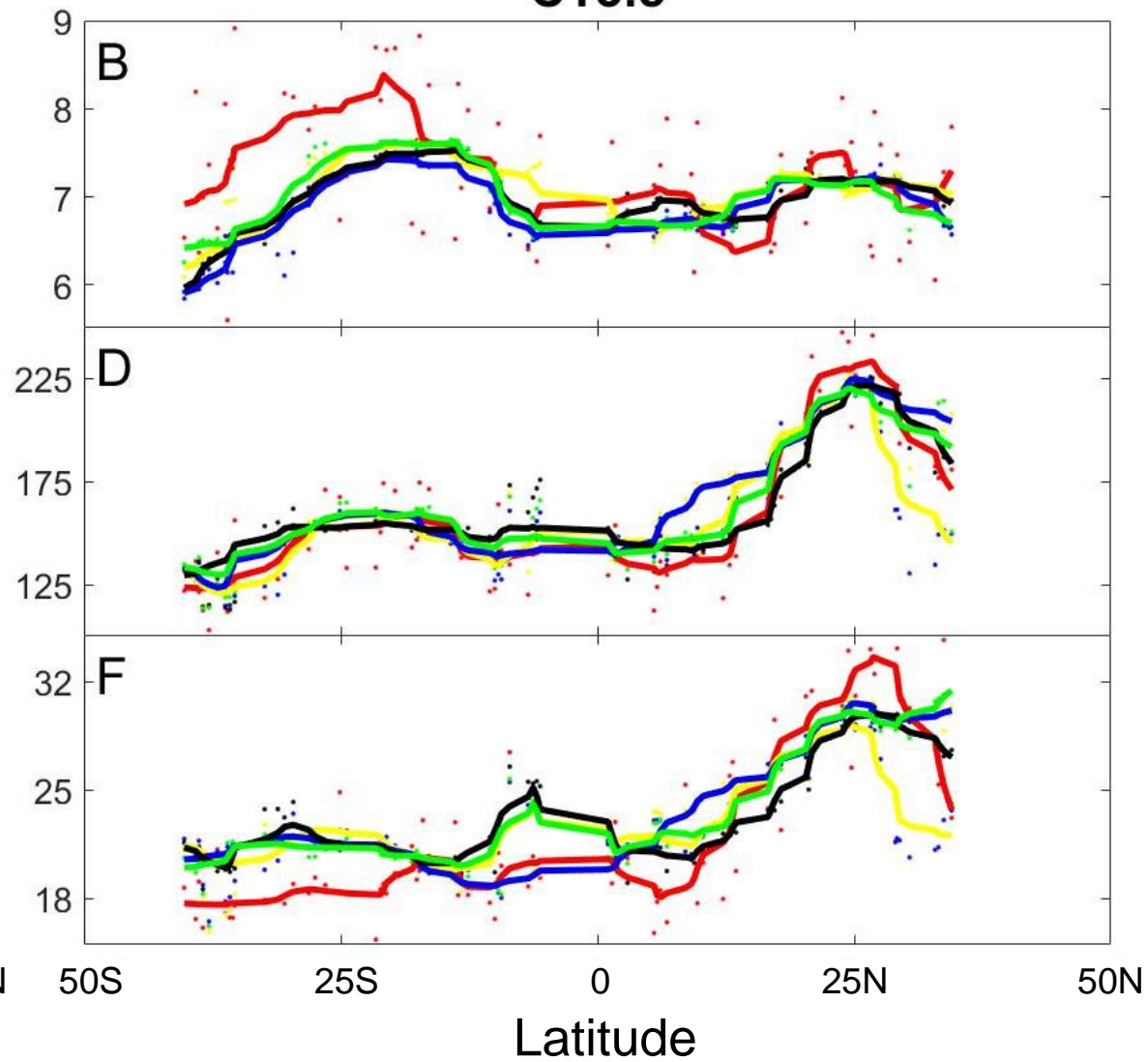


Figure 5.

AMT28**C13.5**

• In situ • Spring • Summer • Autumn • Winter